MJFAS
Malaysian Journal of Fundamental and Applied Sciences

Nasution *et al.* | Malaysian Journal of Fundamental and Applied Sciences, Vol. 22 (2026) 1079–1095

RESEARCH ARTICLE

Bioactive Compound from *Nypa fruticans* Endophytic Fungi: Isolation, Identification, Biological Screening, and *In Silico* Studies

Sakinah Salman Ahmad Nasution[a], Elfita[b,*] Hary Widjajanti[c], Ferlinahayati[b], Sofa Fajriah[d]

[a]Graduate School of Sciences, Faculty of Mathematics and Natural Sciences, Sriwijaya University, South Sumatra 30129, Indonesia, [b]Department of Chemistry, Faculty of Mathematics and Natural Sciences, Sriwijaya University, South Sumatera 30662, Indonesia, [c]Department of Biology, Faculty of Mathematics & Natural Sciences, Sriwijaya University, South Sumatera 30662, Indonesia, [d]Research Center for Pharmaceutical Ingredients and Traditional Medicine, National Research and Innovation Agency (BRIN), KST Soekarno, Cibinong, West Java

Abstract *Nypa fruticans* is one of the unique and dominant mangrove species of tropical coastal areas that is traditionally used for the treatment of many different illnesses. The objective of this study was to isolate and identify bioactive secondary metabolite from endophytic fungi from trunk of *Nypa fruticans*. The investigation included the isolation and morphological identification of endophytic fungi, followed by ethyl acetate extraction. The crude extracts were screened for antibacterial activity by disc diffusion method and antioxidant potential by DPPH assay. Purification of the highly active Diaporthe sp. (Nb3) extract by column chromatography yielded a pure crystalline compound, which was elucidated by 1D/2D NMR and mass spectrometry as 5-hydroxy-4-(hydroxymethyl)-2H-pyran-2-one (compound 1). Compound 1 showed a significant antioxidant scavenging activity under our assay conditions (IC_{50} = 70 µg/mL) and moderate antibacterial activity against *Escherichia coli* (MIC 125 µg/mL), *Salmonella typhi* (MIC 125 µg/mL), *Staphylococcus aureus* (MIC 250 µg/mL) and *Bacillus subtilis* (MIC 250 µg/mL). To rationalize these biological networks, comprehensive in silico screens were performed. PASS Online profiling predicted high probabilities (Pa>0.800) for NADPH peroxidase and glucan endo-1,6-beta-glucosidase inhibition with an excellent ADMET profile characterized by high gastrointestinal absorption and zero Lipinski violations. Molecular docking analysis also showed spontaneous binding configurations (ΔG≤-5.0 kcal/mol) on 12 targeted receptors. These dual mechanisms were stabilized by strong binding affinity toward the antibacterial target tyrosyl-tRNA synthetase (PDB ID: 1JIJ, Δ

G=−6.2 kcal/mol) and key cytoprotective regulators such as lipoxygenase (PDB ID: 1DGH, ΔG=−6.0 kcal/mol). The computational alignment ultimately confirms the isolated compound as a potent therapeutic lead candidate.

Keywords: *Nypa fruticans*, endophytic fungi, antibacterial, antioxidant, molecular docking.

***For correspondence:**
elfita_kimia@unsri.ac.id

Received: 4 August 2026
Accepted: 15 September 2026

© Copyright Nasution. This article is distributed under the terms of the Creative Commons Attribution License, which permits unrestricted use and redistribution provided that the original author and source are credited.

Introduction

The urgency of addressing antimicrobial resistance (AMR) is becoming increasingly critical as it poses a significant global health threat. The development and spread of antimicrobial resistant (AMR) infections have increased to frightening levels, with resistant pathogens such as *Staphylococcus aureus*, *Klebsiella pneumoniae*, *Enterobacter* spp., and *Pseudomonas aeruginosa* linked to high mortality rates globally. The World Health Organization (WHO) has listed AMR as one of the top three threats to human health and AMR was estimated to be responsible for 4.95 million deaths in 2019, of which 1.27 million deaths

were directly attributable to bacterial resistance [1], [2], [3], [4]. The development of “superbugs” or pathogens resistant to most known antibiotics is progressing rapidly and needs rapid action. AMR threatens to create a post-antibiotic era with few new antimicrobial drugs under development and increasing global demand for treatment. The growing difficulty of managing infections highlights the necessity of effective interventions to reduce the risk of severe illness and death. These include better surveillance, cutting back on unneeded antibiotic use, antimicrobial stewardship and new drug and vaccine research. The future of modern medicine is at risk unless coordinated global efforts are made [5], [6].

In addition to treating AMR, antioxidants also play a role in protecting the body from oxidative stress by reactive oxygen species (ROS). This oxidative stress is linked to a number of diseases such as cancer, cardiovascular diseases and neurodegenerative diseases like Alzheimer’s. Antioxidants neutralise free radicals by donating electrons, thereby preventing cellular damage and promoting health. Natural antioxidants especially obtained from plant sources are generally preferred to synthetics due to their safety and other health benefits. They contain vitamins, polyphenols, flavonoids and carotenoids, which fight oxidative stress, as well as contribute to general metabolic health. For example, polyphenols have been associated with anti-inflammatory and antioxidant properties that reduce the risk of chronic disease. Also, natural antioxidants are gaining importance in food preservation, since they are used to preserve the shelf life by oxidation. Nevertheless, over-consumption of some antioxidants such as vitamins C and E can exhibit pro-oxidant effects under certain conditions, highlighting the need to look for balanced and safe sources [7], [8], [9], [10], [11].

Endophytic fungi are symbiotic microorganisms living in plant tissues without causing any damage to the host plant, and they have been recognised as promising sources of bioactive compounds. These fungi are present in almost all plant species, and they produce secondary metabolites, which often show promising pharmacological activities, including antibacterial, antioxidant, antimicrobial, and anticancer activities. Through their long co-evolution with plants, endophytes contribute to plant growth and stress resistance while producing compounds such as alkaloids, flavonoids, and terpenoids, which have medical applications. Notably, some endophytes have provided critical compounds for drug development, such as the anticancer agent paclitaxel derived from *Taxomyces andreanae* [12], [13], [14], [15]. This makes endophytic fungi a promising area of study for the discovery of new therapeutic agents.

The mangrove palm *Nypa fruticans* plays a crucial ecological role in coastal protection and sediment stabilization, while its traditional medicinal use includes treating fever, diabetes, and hypertension. Given its ecological importance and local population declines, harvesting large amounts of *N. fruticans* biomass for chemical extraction poses ecological risks. [16], [17]. Endophytic fungi inhabiting *N. fruticans* with over 153 species reported across Southeast Asia offer a sustainable alternative for bioactive compound discovery without harming wild plant stands. However, despite their rich diversity, the specific bioactive metabolites produced by these endophytes remain understudied, highlighting the need to explore their chemical and pharmacological potential [18], [19], [20].

Antimicrobial resistance (AMR) remains a major global health threat that requires ongoing discovery of new therapeutic agents. At the same time, natural antioxidants acquired from endophytic fungi have excellent prospects in alleviating oxidative stress and promoting general cellular health. Endophytic fungi especially from mangrove ecosystems such as *Nypa fruticans* are rich reservoirs of different bioactive scaffolds to fight infectious and oxidative damage related conditions. Incorporating these naturally occurring metabolites in modern drug discovery is a sustainable way to address the increasing health issues. In this study, we evaluated the baseline antibacterial activity of metabolites isolated from *Nypa fruticans* endophytes against standard reference pathogens to establish their initial bioactivity profile and molecular mechanisms.

But screening this diverse set of metabolites in the traditional lab-based way is often time-consuming and resource-intensive. In silico molecular docking analysis has emerged as a game changer in modern drug discovery to bridge this gap. This computational approach provides deep mechanistic insights at molecular scale through the simulation of the interaction between bioactive compounds and specific biological targets. In context of antimicrobial research, targeting essential bacterial proteins like Tyrosyl-tRNA synthetase (PDB ID: 1JIJ), Methionyl-tRNA synthetase (PDB ID: 1TVF), Dihydrofolate reductase (PDB ID: 3SRW), DNA gyrase B (PDB ID: 1KZN), Penicillin-binding protein (PDB ID: 5OJ0) and Glucosyltransferase B (PDB ID: 8FKL) provides a way to identify compounds that can effectively inhibit bacterial protein synthesis, DNA replication and cell wall synthesis.

Furthermore, the antioxidant potential can be explored to a great extent by in silico profiling against a wide variety of human proteins. Targets such as Xanthine oxidase (PDB ID: 1XAN) and Catalase (PDB

ID: 1DGH) can be used to evaluate the prevention and neutralisation of reactive species, whereas Peroxiredoxin 5 (PDB ID: 4K7O) and Keap1 (PDB ID: 4ZY3) can give insight into cellular protection and activation of endogenous defence pathways. Moreover, the molecular docking against Human Glutathione Peroxidase 7 (PDB ID: 2P31) and Carbonic Anhydrase I (PDB ID: 5GMM) greatly extends the pharmacological spectrum for exhaustive antioxidant and cellular cytoprotective applications. In this context, the present study combines in vitro assays with a broad multi-target in silico approach to provide insight into the therapeutic landscape of secondary metabolites produced by *Nypa fruticans* endophytic fungi, establishing a solid basis for the discovery of new high-affinity antimicrobial and antioxidant agents.

Materials and Methods

Plant sample collection and preparation

Nypa fruticans mangrove specimens were gathered from the Sungsang IV region in South Sumatra (coordinates: 2º 20' 58" N, 104° 54' 22" E). These samples were later identified at GENBINESIA (Generasi Biologi Indonesia) number: BT-072478.

Endophytic fungi isolation

The trunk was washed in running water. The samples were sterilised by placing them under Laminar Air Flow hood (Esco Lifesciences, LVG-4AG-F8) and soaking in 70% ethanol (C_2H_6O) and rinsed with distilled water. Afterwards the trunk was immersed in sodium hypochlorite (NaOCl) and then in sterile distilled water. Sterilised samples were aseptically sliced and placed on Potato Dextrose Agar (PDA) plates containing chloramphenicol and incubated at room temperature for 3 to 7 days. Daily observations were made until fungal growth appeared. The fungal colonies were subcultured onto fresh PDA plates and incubated for several days until pure colonies were obtained [21], [22].

Characterization and identification of endophytic fungi

The purified fungal strains were subsequently transferred to PDA medium for detailed macroscopic and microscopic analysis. Macroscopic characteristics were focusing on color, texture, radial lines, concentric rings, and exudate droplets. Microscopic examination was conducted using Henrici's slide culture method using Hirox 1000 digital microscope. Identification was carried out by comparing the macroscopic and microscopic features with existing literature [23], [24].

Cultivation and extraction of endophytic fungi

Fungal colonies growing on the surface of the PDA medium were transferred onto fresh PDA medium to obtain pure cultures using mycelial fragments. The transferred cultures were incubated untill good developed colonies were formed. The endophytic fungus was then cultured in fifteen 1-L glass bottles, each containing 350 mL of Potato Dextrose Broth (PDB). 15 mycelial plugs (5 mm in diameter, cut with a cork borer) were inoculated into each bottle. The cultures were maintained in static conditions, at room temperature, for four weeks. After incubation, the broth was extracted using ethyl acetate. The concentrated extract was dried in an oven at 40°C until constant weight was obtained (±24 h).

Antibacterial and Antioxidant Activity Assays

The antibacterial activity of the endophytic fungi extracts (4% in DMSO) was evaluated using the disk diffusion method on nutrient agar (NA) against *Staphylococcus aureus* (ATCC 25923), *Escherichia coli* (ATCC 25922), *Bacillus subtilis* (ATCC 6633), and *Salmonella typhi* (IPCCCB.11.669) with three replications. Tetracycline and DMSO were used as positive and negative controls, respectively. After 24 hours of incubation at 37°C, the inhibition zone diameters were measured and compared to the standard antibiotic. Concurrently, the antioxidant activity was assessed using the DPPH radical scavenging method. Extracts (1 mL) at various concentrations (500 - 7.8125 µg/mL) were mixed with 3 mL of 62.5 µM DPPH solution, incubated in the dark for 30 min, after that the decrease in absorbance was measured at wavelength of 517 nm by using UV-vis spectrophotometer (Thermo Scientific Genesys 150). The percentage of free radical scavenging activity was calculated [25], [26].

Isolation and identification of chemical compounds

The ethyl acetate extract of Nb3 (900 mg) was subjected to silica gel column chromatography (CC) via dry loading. The column was packed with 45 g of silica gel 60G (70–230 mesh) as the stationary phase. Elution was performed in a stepwise gradient manner using n-hexane: ethyl acetate (10:0 to 0:10, v/v), followed by 100% methanol. Fractions (10 mL each) were collected and monitored by TLC (n-hexane: ethyl acetate, 5:5 v/v). Fractions with similar TLC profiles were pooled and concentrated to yield seven major fractions: F1 (56 mg), F2 (47 mg), F3 (36 mg), F4 (84 mg), F5 (238 mg), F6 (152 mg), and F7 (104

mg). Fraction F6 (152 mg) was further purified by open column chromatography over silica gel 60G (10 g) using a stepwise gradient manner of n-hexane: ethyl acetate (10:0 to 0:10, v/v) and 100% methanol. Based on TLC monitoring, similar eluates were combined to give two subfractions, F6.1 (37 mg) and F6.2 (16 mg). Subfraction F6.1 yielded clear crystals (37 mg), which showed a single spot on TLC after visualization with cerium sulfate spraying, confirming its purity. The isolated compound was subsequently characterized using 1D, 2D NMR (Bruker Ascend 700 MHz) and mass spectrometry (Agilent 6545 Q-TOF LC/MS). High-resolution mass spectra were acquired in both positive (ESI^+) and negative (ESI^-) ionization modes over a mass scan range of m/z 100–1500 using Agilent MassHunter Workstation Software.

In Silico Bioactivity Prediction Using PASS Online

The bioactivity spectrum of the isolated compound was predicted using the PASS Online web (https://way2drug.com/PassOnline/) server by submitting its Canonical SMILES string (C1=C(C(=COC1=O)O)CO). Potential targets were selected based on the probability of being active (P_a) and inactive (P_i), focusing on values where $P_a > 0.7$.

Molecular Docking Simulation and Binding Analysis

Molecular docking was performed against twelve target proteins retrieved from the RCSB Protein Data Bank (https://www.rcsb.org/) in Protein Data Bank (PDB) format, including 1JIJ, 1TVF, 3SRW, 5MMN, 5OJ0, 8FKL, 1XAN, 4K7O, 5GMM, 4ZY3, 1DGH, and 2P31. Target structures were prepared by BIOVIA Discovery Studio 2025 to removing water molecules and add polar hydrogens, and the prepared structures were subsequently saved in .pdb format. The 3D structure of Compound 1 and the native/reference ligands were obtained in Structure Date File (SDF) format directly from PubChem (https://pubchem.ncbi.nlm.nih.gov/). To accommodate ligands with unknown binding sites, blind docking was carried out across the entire surface of each target protein. The search grid box was defined with adequate dimensions to cover the whole protein structure without bias. Docking simulations were executed using PyRx software (version 0.8) to determine binding affinities (ΔG, kcal/mol) [27]. The 2D and 3D ligand-receptor interactions were visualized using PyMOL (version 3.1) [28] and BIOVIA Discovery Studio 2025 [29].

Drug-likeness and ADME Profiling

Physicochemical properties, pharmacokinetic profiles (ADME), and drug-likeness parameters were evaluated using the SwissADME web tool (http://www.swissadme.ch/). The canonical SMILES notations (C1=C(C(=COC1=O)O)CO) of the target compounds were retrieved and inputted into the server to generate the corresponding ADME profiles and drug-likeness evaluations. Key descriptors assessed included molecular weight (MW), TPSA, hydrogen bond donors/acceptors, lipophilicity (Consensus Log Po/w), gastrointestinal (GI) absorption, Cytochrome P450 enzyme inhibition, and compliance with Lipinski's Rule of Five and PAINS structural filters.

Antibacterial and antioxidant test of pure compound

The pure compounds obtained were tested for antibacterial activity to determine the Minimum Inhibitory Concentration (MIC) for purified compounds, and tested within concentrations ranging from 1000 to 3.91 µg/mL. The MIC value was determined by measuring the size of the inhibition zone, which exceeded 7 mm, indicating the presence of antibacterial activity at the corresponding concentration. For the antioxidant test, the DPPH method was employed and measured using a UV-Vis spectrophotometer (Thermo Scientific Genesys 150) at a wavelength of 517 nm, followed by the calculation of the IC_{50} value [30], [31].

Results and Discussion

Endophytic fungi isolated from trunk of *N. fruticans*

Isolation was conducted on the trunk of *Nypa fruticans*, resulting in three isolates were coded as Nb1 to Nb3. Macroscopic identification was carried out for each isolate, and the results are shown in Table 1. The microscopic descriptions and characteristics are provided in Table 2. Based on the macroscopic and microscopic data, three different genera were identified from the trunk of *N. fruticans*, namely *Pythium* (Nb1), *Pestalotiopsis* (Nb2), and *Diaporthe* (Nb3). Macroscopic and microscopic images of the three isolates can be seen in Figure 1.

Table 1. Macroscopic characteristics of endophytic fungi isolated from trunk of *N. fruticans*.

Code	Surface Colony	Reverse Colony	Structure	Elevation	Pattern	Exudate Drops	Radial line	Concentric circle
Nb1	White to gray	Dark gray to blackish	Cottony	Flat	Circular	-	√	-
Nb2	White margin with dark gray	Blackish with lighter edge	Cottony	Flat	Circular	-	√	-
Nb3	White fluffy	Pale orange to yellow	Cottony	Raised	Rosette	-	-	-

Note: "-" indicates the absence of the corresponding morphological feature (exudate drops, radial lines, or concentric circles).

Previous research conducted in Southeast Asia identified *Pestalotiopsis* as one of the endophytic fungi found in *Nypa fruticans*. However, other genera such as *Pythium* and *Diaporthe* were not recorded [19]. Meanwhile, a study conducted in Indonesia successfully identified 18 endophytic fungal isolates from 12 different genera, including *Aspergillus*, *Diaporthe*, *Penicillium*, *Apophysomyces*, *Paecilomyces*, *Humicola*, *Nodulisporium*, *Fusarium*, *Mortierella*, *Papulaspore*, *Pestalotiopsis*, and *Cladosporium* [18]. These findings emphasize that environmental conditions can influence the types of fungi that develop on the plant, indicating significant differences in fungal diversity based on location and microhabitat conditions.

Table 2. Macroscopic characteristics of endophytic fungi isolated from trunk of *N. fruticans*.

Code	Spore	Shape	Hyphae	Characteristic	Species of Identification
Nb1	Oospore	Globose	Non-septate	Coenocytic hyphae, oogonia with oospores	*Pythium* sp.
Nb2	Conidia	Ellipsoid	Septate	Conidia formed in acervuli with setae	*Pestaloptiosis* sp.
Nb3	Conidia	Fusiform	Septate	Conidiophores simple, curved conidia	*Diaporthe* sp.

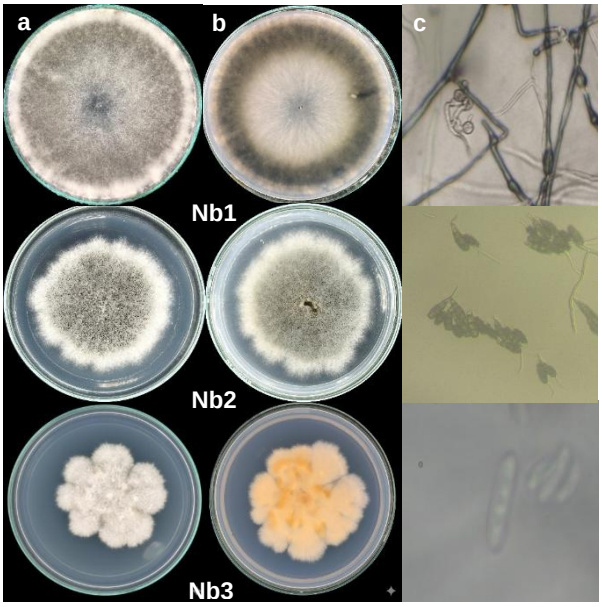


Figure 1. Morphological characteristics of the endophytic fungi isolated from trunk of *N. fruticans*. (a) Front view of macroscopic colony growth on PDA. (b) Reverse view of macroscopic colony growth on PDA. (c) Microscopic structures observed via Henrici's slide culture on PDA at 1000x magnification.

Antibacterial and antioxidant activity of endophytic fungi extracts

The results of the study showed that the samples tested exhibited varying antibacterial and antioxidant activities depending on their genus. Sample Nb3 (Diaporthe sp.) demonstrated consistent moderate antibacterial activity (50–70%) across all tested pathogens. Against E. coli, Nb3 showed an activity of 56.33 ± 0.31 µg/mL, comparable to the moderate effect of Nb1 (Pythium sp.) at 55.79 ± 0.32 µg/mL. Furthermore, Nb3 exhibited moderate inhibition against S. aureus (52.21 ± 1.55 µg/mL) and S. typhi (65.13 ± 1.40 µg/mL). Varied profiles were noted against B. subtilis, where both Nb1 (58.42 ± 0.45 µg/mL) and Nb3 (53.52 ± 2.10 µg/mL) were classified as moderately active.

Table 3. Antibacterial and antioxidant properties of endophytic fungi extract's isolated from trunk of *N. fruticans*.

Sample	Extract Yield (mg)	Genus	Antibacterial activity (% relative to control)				Antioxidant activity (IC_{50}, µg/mL)
			E. coli	*S. aureus*	*S. thypi*	*B. subtilis*	
Nb1	835	*Pythium* sp.	55.79 ± 0.32 **	50.60 ± 0.15 **	34.82 ±0.55 *	58.42 ± 0.45 **	350.94**
Nb2	1400	*Pestaloptiosis* sp.	46.46 ± 0.25 *	39.98 ± 0.05 *	43.16 ± 1.15 *	47.57 ± 0.75 *	282.92**
Nb3	900	*Diaporthe* sp.	56.33 ± 0.31 **	52.21 ± 1.55 **	65.13 ± 1.4 **	53.52 ± 2.10 **	27.34***
Positive Control		Ascorbic acid					10.72****
		Tetracyclin	100***	100***	100***	100***	

Note: Antibacterial activity percentage: ***: >70% (strong), **: 50-70% (moderate), *: <50% (weak).
Antioxidant activity IC_{50} (µg/mL): ****very strong < 20 µg/mL; ***strong 20 - 100 µg/mL; **moderate 100 - 500 µg/mL; * weak > 500 µg/mL.

In terms of antioxidant activity, the IC_{50} value was utilized to evaluate the radical scavenging potency of the fungal extracts. Notably, sample Nb3 demonstrated a highly prominent antioxidant capacity with a remarkably low IC_{50} value of 27.34 µg/mL, classifying it as a strong antioxidant agent as it comfortably falls within the established 20–100 µg/mL threshold. In sharp contrast, the other fungal extracts exhibited significantly lower potencies, with sample Nb1 and sample Nb2 yielding substantially higher IC_{50} values of 350.94 µg/mL and 282,92 µg/mL respectively. When benchmarked against ascorbic acid as the positive control, which exhibited a very strong antioxidant activity with an IC_{50} value of 10.72 µg/mL, sample Nb3 displayed exceptional therapeutic potential compared to the other tested endophytes.

The strategic selection of Nb3 for subsequent chromatographic isolation is highly justified by these findings. Nb3 exhibited the most exceptional and balanced dual-action profile, pairing its superior antioxidant capacity with very potent, broad-spectrum antibacterial activity against *Escherichia coli*, *Staphylococcus aureus*, *Salmonella typhi*, and *Bacillus subtilis*. Consequently, sample Nb3 possesses the most holistic pharmacological potential for further development. The comprehensive screening data for both antibacterial and antioxidant activities are summarized in Table 3.

Isolation and identification of chemical compound

The ethyl acetate extract (900 mg) of Nb3 was separated and purified to obtain a clear crystal (37 mg). Performed spectroscopic analysis (NMR 1D and 2D) to determine the compound's molecular structures that were isolated. ^{1}H-NMR (CD_3OD, 700 MHz) δ_H ppm values and ^{13}C-NMR (CD_3OD, 175 MHz) δ_C ppm values of the compound were shown in table 4.

The ^{1}H-NMR spectrum shown in Figure 2 reveals three proton signals that can be grouped based on their chemical environments. Two proton signals were detected at δ_H 7.75 (1H, s) and 6.30 (1H, s) ppm, with each signal indicating the absence of strong chemical interactions (singlet signals). Furthermore, one proton signals were detected at 4.21 (2H, s) ppm, all of which correspond to protons attached to carbon atoms adjacent to oxygen atom. This signal indicate that the protons are in a chemical environment influenced by the presence of oxygen, most likely from hydroxyl, ether, or other oxygen-containing functional groups.

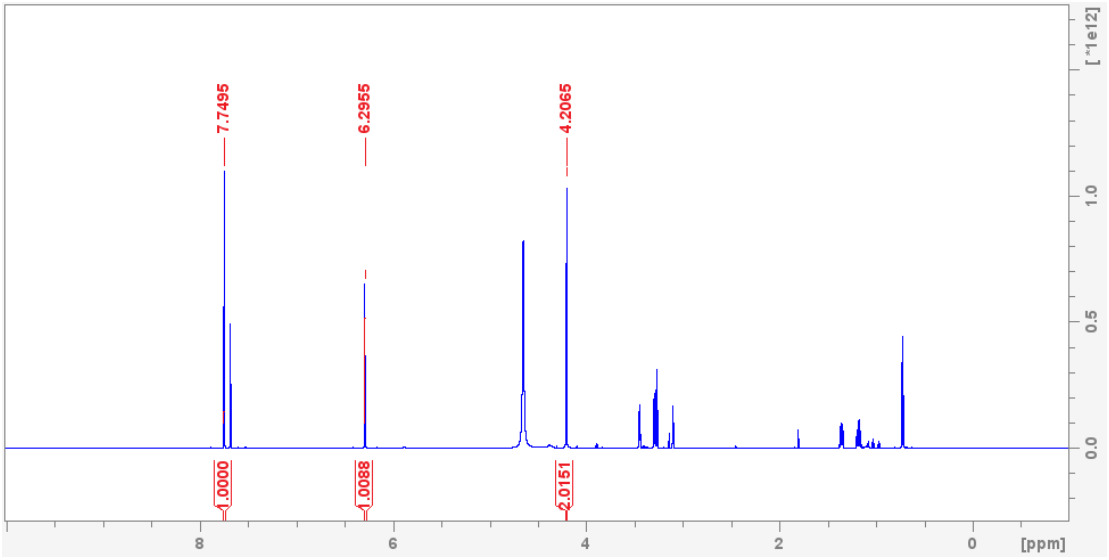


Figure 2. The ^{1}H-NMR spectra of compound 1 (CD_3OD, 700 MHz).

The ^{13}C-NMR spectrum shown in Figure 3 reveals a total of 6 carbon signals, which can be grouped based on their respective chemical environments. Among these signals, four can be identified as aromatic carbons or keton or oxygen-containing functional groups, appearing at δ_C 166.8, 143.7, 137.4, and 107.1 ppm. There is also a carbonyl ester signal detected at δ_C 173.2 ppm, indicating the presence of an ester group in this compound, commonly detected in this chemical range. Furthermore, the spectrum shows one carbon signal bound to heteroatoms or oxygenated carbons, identified at δ_C 57.5 ppm. Based on the positions and patterns of these signals, it can be inferred that the compound's structure contains functional groups involving oxygen, such as alcohol or ether. Overall, this ^{1}H-NMR and ^{13}C-NMR spectrum provides a clear depiction of the analyzed compound's structure, may showing the presence of carbonyl ester groups, and oxygen-containing functional groups.

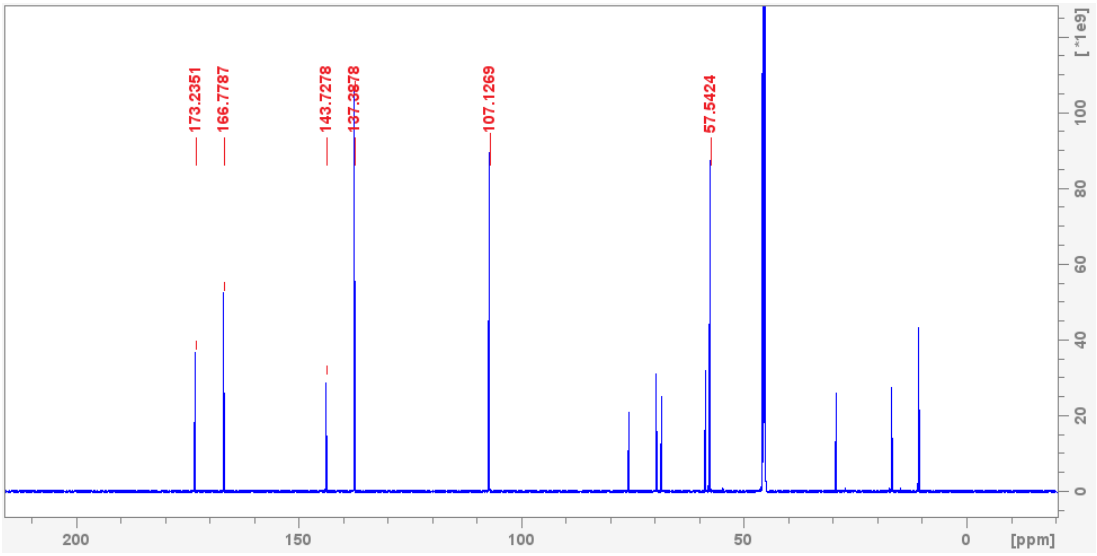


Figure 3. The ^{13}C-NMR spectra of compound 1 (CD_3OD, 175 MHz).

To gain a deeper understanding of the compound's structure, an analysis using HSQC (Heteronuclear Single Quantum Correlation) technique was performed, as shown in Figure 3. This technique allows for the identification of direct correlations between protons (^{1}H) and carbons (^{13}C) in the compound. The HSQC (Heteronuclear Single Quantum Coherence) spectrum (Figure 4) obtained shows correlations between protons and carbons that are related to each other in various chemical environments. In the HSQC, the signals detected at δH 7.75 ppm showed a clear correlation with the carbon signal at δC 137.4 ppm, while the signal at δH 6.30 ppm correlated with δC 107.1 ppm. These interactions confirmed

the presence of sp2 hybridized carbons in the compound's structure. A proton signal at δ_H 4.21 ppm correlates with carbon at δ_C 57.5 ppm.

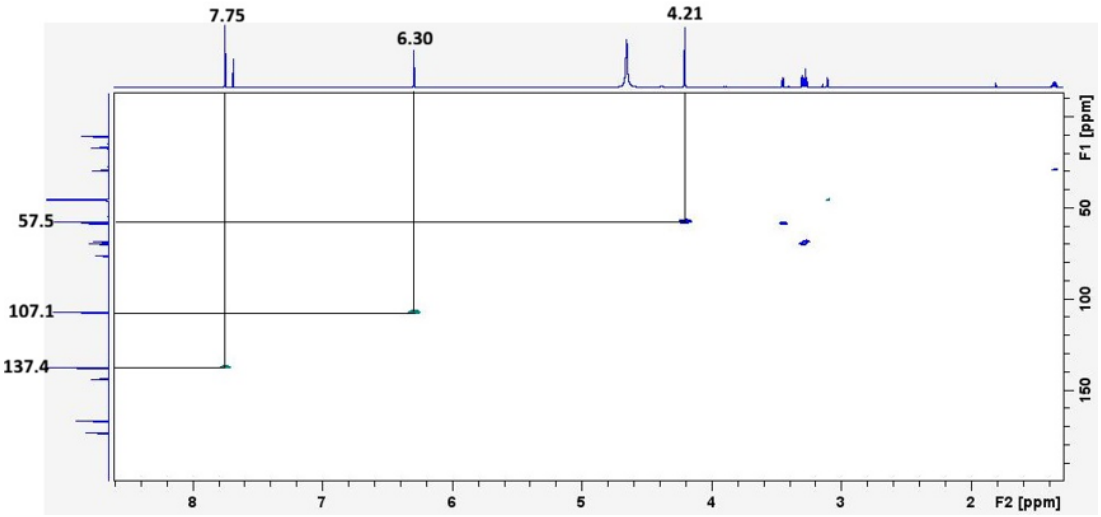


Figure 4. The HSQC spectral of compound 1.

An analysis using the HMBC (Heteronuclear Multiple Bond Correlation) technique was also performed, which allows observation of correlations between protons and carbons connected through two or more bonds. The HMBC spectrum obtained provides important information about more distant proton-carbon interactions within the compound's structure. The HMBC spectrum (Figure 5), two proton signals at δH 7.75 and 6.30 ppm showed long-range correlations with the quaternary carbon signals at δC 143.7, 166.8, and 173.2 ppm, indicating that both methine protons are located in the immediate vicinity of an ester carbonyl group and two oxygenated olefinic carbons. Moreover, the cross-peak of the proton at δH 7.75 ppm to the carbon at δC 107.1 ppm confirmed their mutual proximity within the unsaturated core. Importantly, the proton at δH 6.30 ppm showed a diagnostic correlation with the aliphatic carbon at δC 57.5 ppm, showing that an oxymethylene group is directly attached to this particular position of the core ring. This substitution was supported by the methylene proton signal at δ H 4.21 ppm (δ C 57.5 ppm), which gave strong HMBC correlations back to the core carbons at δ C 166.8 and 107.1 ppm. The entire connectivity of the structural fragments was mapped out by the set of heteronuclear networks, which allowed us to assign the entire framework of the compound 1.

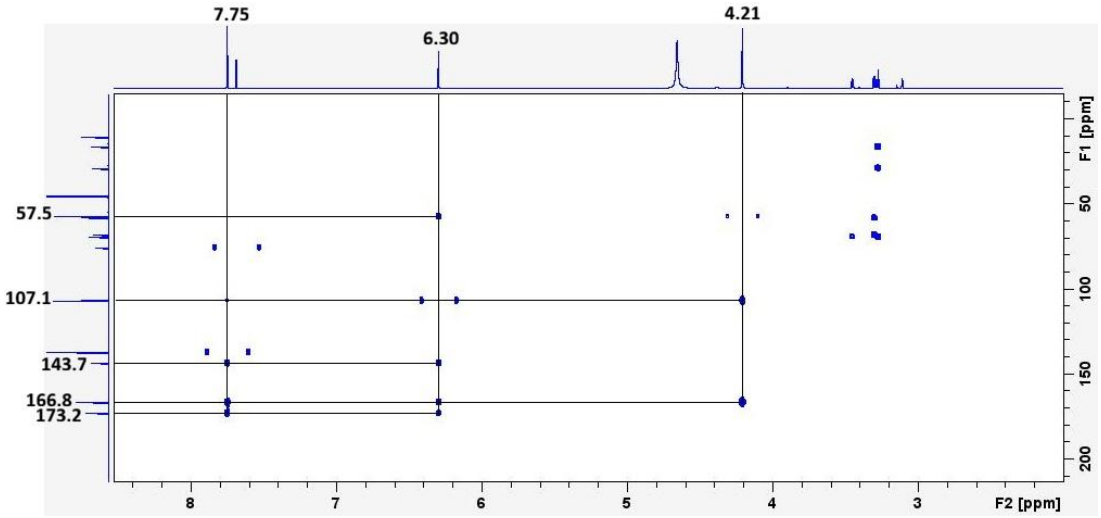


Figure 5. The HMBC Spectral of Compound 1.

Overall, the HMBC analysis provides a more detailed picture of the long-range proton-carbon relationships, helping to map the molecular structure more thoroughly and confirming the interactions between functional groups in the compound. This technique complements the results of the HSQC and ^{1}H-NMR analyses, providing a more comprehensive understanding of the molecular structure and the interconnections between the groups in the compound being analyzed.

Table 4. NMR 1D and 2D spectral data of compound 1

No.	δ_C ppm	Type of C	δ_H pp (ΣH, Multiplicity, Hz)	HMBC
2	173.2	C		
3	107.1	CH	6.30 (1H, s)	57.5; 143.7; 166.8; 173.2
4	143.7	C		
5	166.8	C		
6	137.4	CH	7.75 (1H, s)	107.1; 143.7; 166.8; 173.2
7	57.5	CH_2	4.21 (2H, s)	107.1; 166.8

Compound 1 was obtained as a colorless. Based on the MS analysis using methanol (Figure 6) showed a quasi-molecular ion peak at m/z 143.0337 $[M+H]^+$ (calcd. for $C_6H_7O_4$, 143.0344) and m/z 141.0189 $[M-H]^-$ (calcd. for $C_6H_5O_4$, 141.0188), established the molecular formula of $C_6H_6O_4$ with a mass error of 2.1 ppm and a Double Bond Equivalent (DBE) = 4. This formula consistent with the 5-hydroxy-4-(hydroxymethyl)-2H-pyran-2-one structure.

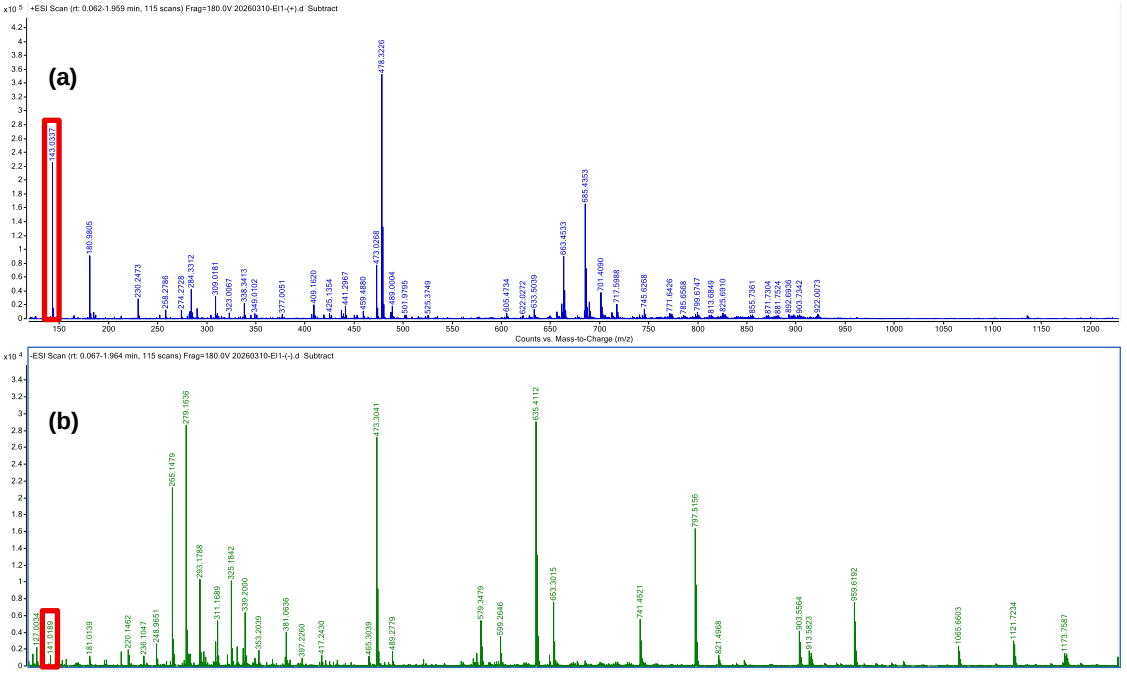


Figure 6. The mass spectra of Compound 1 acquired in (a) positive (ESI^+) and (b) negative (ESI^-) ionization modes. Red boxes highlight the molecular ion peaks and key fragment ions of the target compound.

The 1D and 2D NMR spectral data for compound 1 are shown in Table 4. The molecular structure of compound 1, with carbon atom numbering and HMBC correlations, is shown in Figure 7. Compound 1 contains carbonyl and hydroxyl groups, which impart specific functional characteristics to the compound. Based on extensive 1D and 2D NMR spectroscopic analyses, mass spectrometry data, and thorough

literature dereplication, compound 1 was unambiguously identified as 4-(hydroxymethyl)-5 hydroxy-2H-pyran-2-one. This structural assignment is in complete agreement with the functionalized pyrone derivative previously, which was originally isolated from the marine-derived fungus *Aspergillus flavus* [32]. In addition to the primary resonances attributed to Compound 1, minor signals were observed in both ^{1}H-NMR (δ_H 7.69; 3.45; 3.30; 3.28; 1.37; 1.15 dan 0.73 ppm) and ^{13}C-NMR (δ_C75.8; 69.6; 68.4; 58.6; 29.2; 16.6 dan 10.6 ppm) spectra. These extra signals were identified as trace impurities, as HMBC analysis revealed no structural correlation or connectivity between these peaks and the core molecular framework of Compound 1 and did not match the molecular weight determined by MS analysis.

Although compound 1 is a known chemical entity, our successful isolation of this metabolite from an endophytic fungus (*Diapothe* sp.) associated with the Nipah plant (*Nypa fruticans*) represents a highly significant finding. It not only provides valuable chemotaxonomic insights into the metabolic profile of host-specific endophytes but also demonstrates that this specific chemical scaffold can be biosynthesized across vastly different ecological niches ranging from free-living marine strains to terrestrial mangrove associated symbionts.

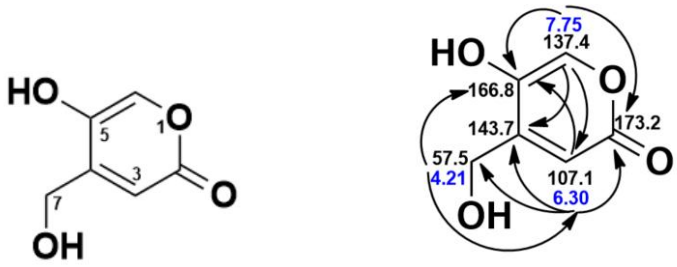


Figure 7. Structure of 4-(hydroxymethyl)-5 hydroxy-2H-pyran-2-one (Compound 1), (A) carbon atom numbering and (B) HMBC correlations.

Biological Activity Spectrum Prediction (PASS Online)

The pharmacological potential of the isolated compound from *Nypa fruticans* endophytic fungi was performed *in-silico* prediction using the Prediction of Activity Spectra for Substances (PASS) Online. This computational tool predicts the biological activity profile of a molecule based on its structural formula, providing the probability of being active (P_a) and inactive (P_i). In this work, $P_a > 0.7$ is considered a good indication that the activity can be experimentally validated, while $0.5 < P_a < 0.7$ indicates that the compound is more likely to show activity but may be different in structure from known drugs in the database. Table 5. Prediction results for compound 1 with a multi-faceted bioactivity profile. Several important targets show P_a values > 0.8 indicating a very high probability of biological effectiveness.

The PASS analysis suggests the compound works as multi-target agents against especially the microbial and oxidative targets. The high P_a value of 0.849 for glucan endo-1,6-beta-glucosidase inhibition and 0.814 for UDP-N-acetylglucosamine 4-epimerase inhibition strongly supports its potential as an antibacterial agent. These enzymes are important for the structural integrity of the bacterial cell wall and biofilm matrix. Inhibition of these pathways is a well-known strategy in the fight against antimicrobial resistance (AMR), as it results in increased osmotic fragility and bacterial cell death [33].

Table 5. Predicted biological activities of the isolated compound using PASS Online.

No.	Biological Activity	P_a	P_i	Pharmacological Potential
1	Aspulvinone dimethylallyltransferase inhibitor	0.886	0.011	Secondary Metabolite Biosynthesis
2	Ubiquinol-cytochrome-c reductase inhibitor	0.880	0.009	Antifungal/Cytotoxic
3	Sugar-phosphatase inhibitor	0.858	0.008	Carbohydrate Metabolism
4	Glucan endo-1,6-beta-glucosidase inhibitor	0.849	0.005	Antibacterial (Cell Wall)
5	NADPH peroxidase inhibitor	0.834	0.008	Antioxidant (Cytoprotective)

6	Methylenetetrahydrofolate reductase inhibitor	0.831	0.014	Antibacterial (Metabolism)
7	UDP-N-acetylglucosamine 4-epimerase inhibitor	0.814	0.005	Antibacterial (Cell Wall)
8	Catechol oxidase inhibitor	0.800	0.003	Anti-melanogenic (Tyrosinase)

Interestingly, the high prediction score for catechol oxidase inhibition (P_a=0.800) further complements the compound's polypharmacological role in modulating oxidative cascades. While catechol oxidases traditionally catalyze the oxidation of phenols into reactive quinones, inhibiting this enzymatic pathway can effectively mitigate the downstream generation of reactive oxygen species (ROS) and cellular browning effects. This mechanism suggests an indirect cytoprotective screening benefit that synergistically enhances the primary radical-scavenging antioxidant capacity of compound 1 [34]**.** To summarise, the PASS Online results represent a strong preliminary validation of the compound dual-action potential. The high consistency of different classes of antimicrobial and antioxidant enzymes provides a good theoretical basis for the follow-up molecular docking study and in vitro biological assays.

Molecular Docking Simulations and Target Identification

Molecular docking simulations were carried out to understand the molecular mechanisms and to predict the binding stability of the compound 1 against the predicted biological targets.

Table 6. Binding energy of compound 1 with 12 different proteins.

Code	Protein	Interaction type					Binding affinity (kcal/mol)
		Hydrogen bond		Hydrophobic	Electrostatic	Unfavorable	
		Hydrogen bond	Carbon hydrogen bond				
a	1JIJ	GLY38, ASP40, THR75, TYR170, GLN196	-	-	-	GLN174	-6.2
b	1TVF	SER75, LYS78, SER116, ASN141	SER263	LEU115, ALA182	-	-	-5.8
c	3SRW	THR47, ASP121, THR122	GLY16, GLY95	-	-	-	-5.4
d	8FKL	SER690	ASP688	-	-	ASP688	-5.2
e	5OJ0	GLN330, TRP324, THR430, ASP431	GLY218	-	-	-	-5.1
f	5MMN	ILE48, GLY75, GLY77, THR165	GLY77	-	-	-	-5.1
g	1DGH	ARG72, PHE132	ARG112	HIS75, ARG112, ALA133	-	-	-6.0
h	5GMM	ASP8, ASN11, HIS64	HIS243	-	-	HIS243	-5.9
i	4ZY3	LEU365, GLY367, VAL465, VAL604, VAL606	GLY417	ALA366	-	GLY367, VAL606	-5.6
j	1XAN	THR57, CYS58, THR339	-	ASP331, ALA342	-	-	-5.8
k	4K7O	GLU16, GLU91, LEU96	VAL94	ALA90, LEU96	-	-	-5.4
l	2P31	LYS36, LYS42, MET114	TYR43	-	-	MET114	-5.1

Table 6 summarises the binding (ΔG) and detailed non-covalent interactions, including conventional hydrogen bonds, carbon-hydrogen bonds, hydrophobic interactions and unfavourable residues. The PASS analysis provided a broad theoretical prediction of potential biological targets of the compound, while the molecular docking simulations were targeted to the most important enzymes that are directly involved in the observed in vitro antibacterial and antioxidant activity. This dual approach enabled us to cross-validate the general biological potential predicted by PASS with detailed residue-level interactions against well-established target proteins.

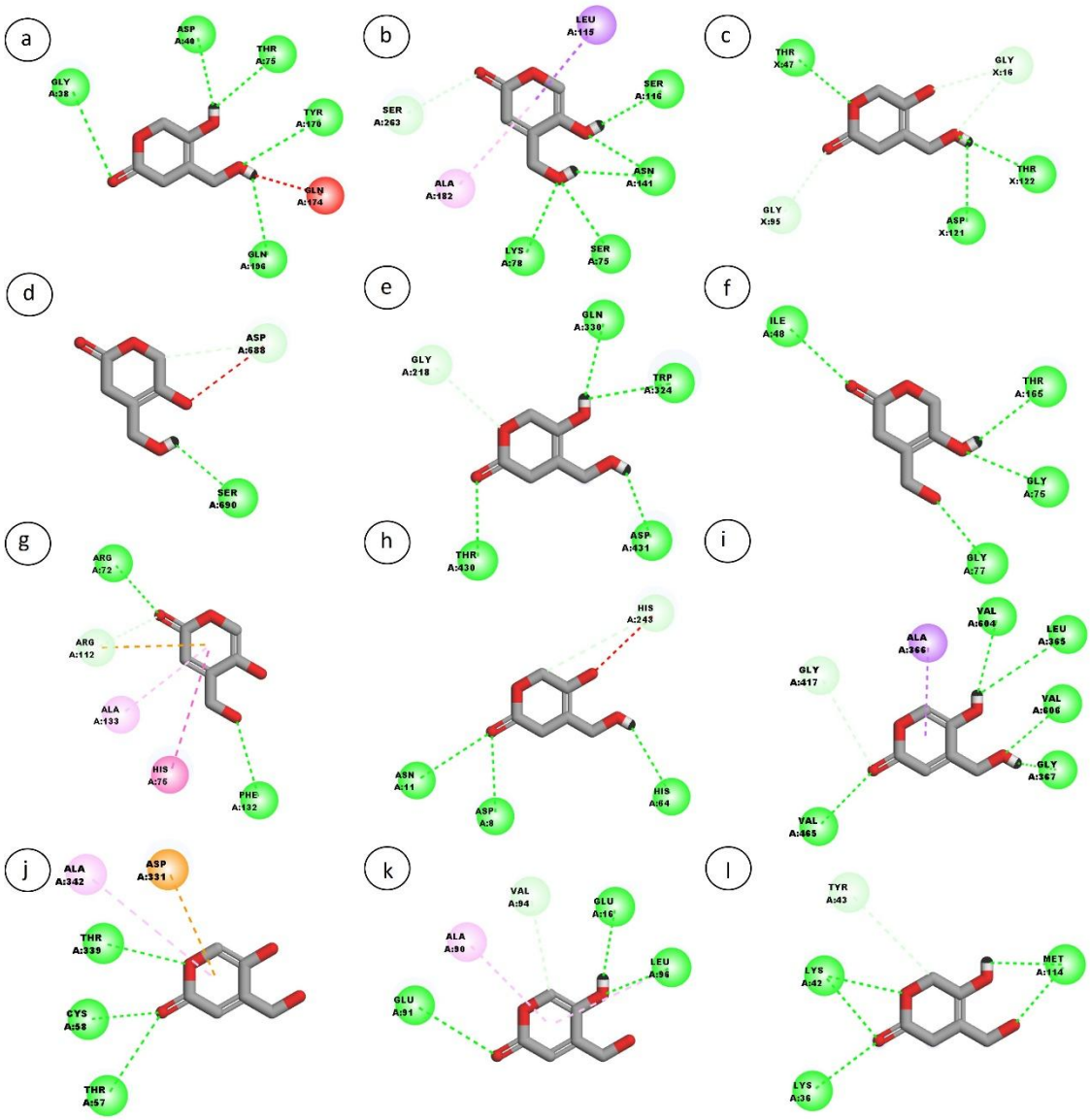


Figure 8. The 2D molecular interaction diagrams of Compound 1 with twelve target proteins: **(a)** 1JIJ, **(b)** 1TVF, **(c)** 3SRW, **(d)** 8FKL, **(e)** 5OJ0, **(f)** 5MMN, **(g)** 1DGH, **(h)** 5GMM, **(i)** 4ZY3, **(j)** 1XAN, **(k)** 4K7O, and **(l)** 2P31. Color codes represent specific interaction types: bright green = conventional hydrogen bonds; light green = carbon-hydrogen bonds; purple/pink/orange = hydrophobic interactions (Pi-Sigma, Pi-Alkyl, or Pi-Pi T-shaped); and red = unfavorable interactions (unfavorable donor-donor or unfavorable acceptor-acceptor).

Compound 1 showed promising binding affinities against several important bacterial enzymatic targets demonstrating its multi-target antibacterial activity. Tyrosyl-tRNA Synthetase (PDB ID: 1JIJ), a key enzyme in bacterial protein synthesis, was the most potent antibacterial target with the strongest binding interaction, with a binding energy of -6.2 kcal/mol. This high affinity is structurally stabilised by five classical hydrogen bonds to the amino acid residues GLY38, ASP40, THR75, TYR170, and GLN196. Although an unfavourable donor-donor interaction between GLN174 (Figure 8a,9a) was observed, the net binding energy is still very favourable. Thus, compound 1 can occupy the active pocket well and may possibly disrupt the aminoacylation process in pathogens such as *Staphylococcus aureus* [35]**.**

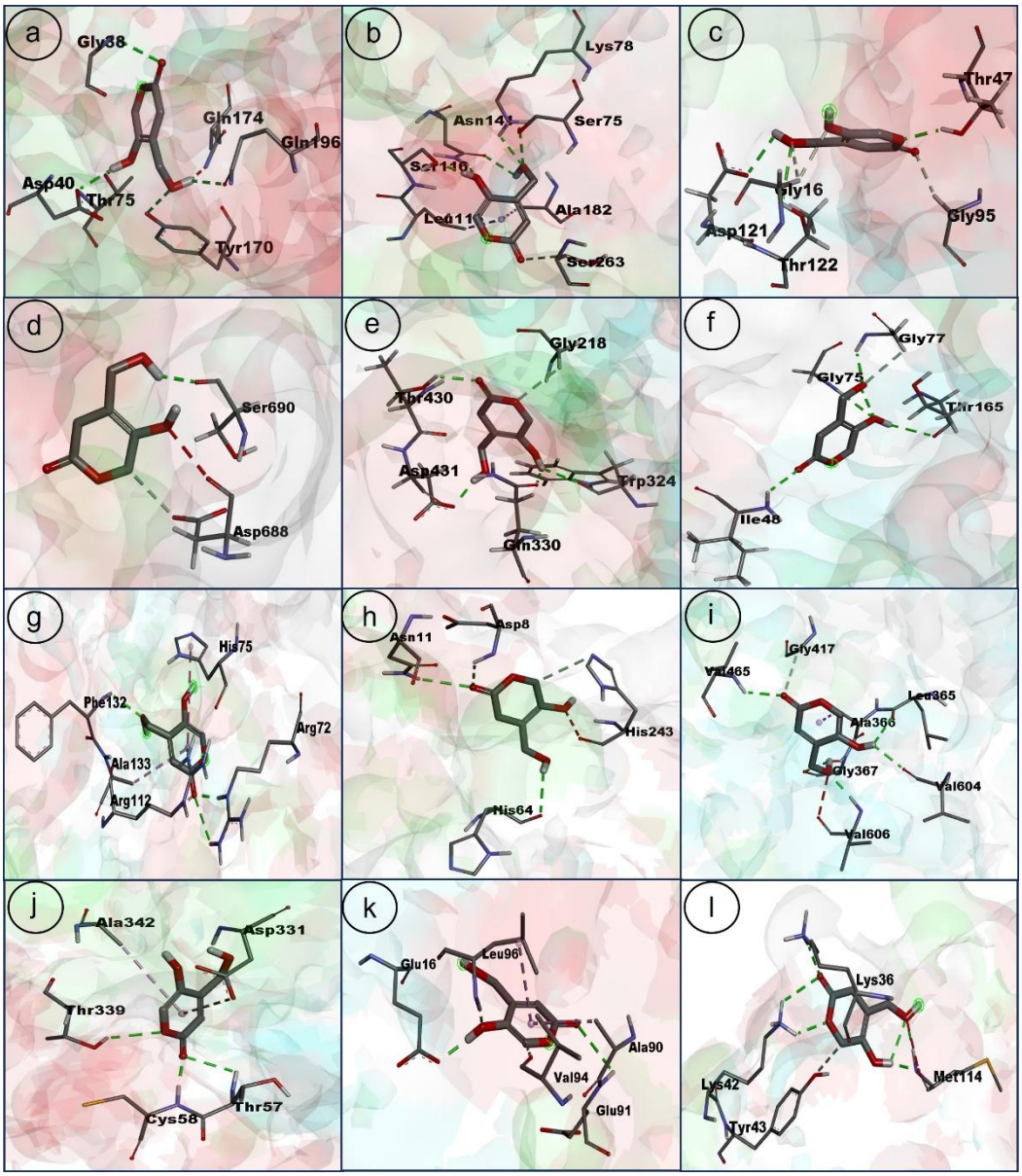


Figure 9. The 3D molecular interaction diagrams of Compound 1 with twelve target proteins: **(a)** 1JIJ, **(b)** 1TVF, **(c)** 3SRW, **(d)** 8FKL, **(e)** 5OJ0, **(f)** 5MMN, **(g)** 1DGH, **(h)** 5GMM, **(i)** 4ZY3, **(j)** 1XAN, **(k)** 4K7O, and **(l)** 2P31. Color codes represent specific interaction types: bright green = conventional hydrogen bonds; light green = carbon-hydrogen bonds; purple/pink/orange = hydrophobic interactions (Pi-Sigma, Pi-Alkyl, or Pi-Pi T-shaped); and red = unfavorable interactions (unfavorable donor-donor or unfavorable acceptor-acceptor).

Furthermore, compound 1 showed strong interaction profiles with enzymes related to the bacterial cell wall integrity and metabolism. The compound exhibited a binding affinity of -5.2 kcal/mol against Glucosyltransferase B (PDB ID: 8FKL) that is important for the formation of dental plaque biofilm and also formed vital hydrogen bonds with SER690, a carbon-hydrogen bond and unfavorable bond with ASP688 (Figure 8d, 9d) [36]. The stable interaction with Dihydrofolate Reductase (PDB ID: 3SRW) at -5.4 kcal/mol, comprising conventional hydrogen bonds with THR47, ASP121, and THR122, and carbon-hydrogen bonds with GLY16 and GLY95 (Figure 8c, 9c) [37], also suggested the disruption of bacterial folate metabolism. Additional metabolic and structural targets such as Methionyl-tRNA Synthetase (PDB ID: 1TVF; ΔG = -5.8 kcal/mol; Figure 8b,9b) [38], Penicillin-Binding Protein (PDB ID: 5OJ0; ΔG = -5.1 kcal/mol; Figure 8e,9e) [39], and 5MMN (ΔG = -5.1 kcal/mol; Figure 8f,9f) [40], further support the compound's ability to act via a synergistic multi-targeted antibacterial mechanism, thus reducing the

probability of rapid resistance development.

Besides its antimicrobial properties, Compound 1 showed excellent binding characteristics against important oxidative stress regulators, in line with preliminary PASS Online predictions. It showed a significant cytoprotective antioxidant capacity, as it interacted with Human Glutathione Peroxidase 7 (PDB ID: 2P31; Figure 8l, 9l), an important enzyme for hydrogen peroxide scavenging, with a stable binding affinity of-5.1 kcal/mol [41]. The compound was docked against Peroxiredoxin 5 (PDB ID: 4K7O; Figure 8k, 9k) to further evaluate its defence mechanisms against oxidative stressors, another important human peroxidase framework and was found to have a strong binding affinity of -5.4 kcal/mol [42]. The stability of the complex in this enzyme is reinforced by a dense network of conventional hydrogen bonds with GLU16, GLU91 and LEU96, a carbon-hydrogen bond with VAL94, and hydrophobic (Pi-Alkyl) bond with ALA90 and LEU96.

In addition, the docking of the compound was also successful in other highly relevant oxidative systems, that are important therapeutic targets to prevent oxidative damage. It exhibited a robust binding energy of −6.0 kcal/mol against Lipoxygenase (PDB ID: 1DGH; Figure 8g, 9g) via specific stabilising interactions, suggesting a high potential to inhibit downstream lipid peroxidation pathways [43]. More favourably, the Xanthine Oxidase Oxidase (PDB ID: 1XAN; ΔG = -5.8 kcal/mol; Figure 8j, 9j), which is responsible for generating reactive superoxide radicals [44], and protein targets 5GMM (ΔG = -5.9 kcal/mol; Figure 8h, 9h) [45] and 4ZY3 (ΔG = -5.6 kcal/mol; Figure 8i, 9i) [46] showed favourable binding geometries and consistent thermodynamic spontaneity. The wide multi-target efficacy of compound 1 suggests that the small molecular framework can dynamically interact with the diverse macromolecular frameworks involved in the redox regulation of human cells.

The thermodynamic profiles of the strongest targets were benchmarked against their respective native co-crystallized ligands to assess the competitive binding efficiency of the isolated metabolite. In the primary antibacterial target Tyrosyl-tRNA Synthetase (1JIJ), compound 1 exhibited a highly spontaneous binding energy of -6.2 kcal/mol, compared to its native structural ligand ([2-amino-3-(4-hydroxy-phenyl)-propionylamino]-(1,3,4,5-tetrahydroxy-4-hydroxymethyl-piperidin-2-yl)- acetic acid) variant which shows a binding affinity of -7.8 kcal/mol. Likewise, for the antioxidant pathway target (1DGH), compound 1 exhibited stable binding configurations (ΔG= -6.0 kcal/mol) compared to its native bulky prosthetic cofactor, protoporphyrin IX (ΔG= -9.6 kcal/mol). The larger molecular weight and highly conjugated ring systems of the native cofactors inherently create a thermodynamic gap, but the compact framework of compound 1 is a highly efficient architecture for establishing specific, targeted binding within the same essential catalytic cavities.

Pharmacokinetic Profile and In Vitro Biological Validation

The physicochemical properties and ADME (Absorption, Distribution, Metabolism, and Excretion) profiles of compound 1 ($C_6H_6O_4$) were evaluated to determine its potential as a drug candidate. The results obtained from the SwissADME platform are summarized in Table 7. The data predict that compound 1 has a very attractive profile as a potential oral drug candidate. Its physicochemical parameters suggest a high structural rigidity and excellent oral bioavailability, supported by a low molecular weight (142.11 g/mol), a TPSA of 70.67 Å², and only 1 rotatable bond.

In addition, the compound has a Consensus Log Po/w of -0.04 and a Log S (ESOL) of -0.70, which are associated with an optimal hydro-lipophilic balance and high-water solubility required for efficient drug absorption. The compound is characterised by high gastrointestinal absorption and is non-permeant to the blood-brain barrier (BBB), decreasing the risk of central nervous system toxicity from a pharmacokinetic point of view. It is not a P-gp substrate (thus resistant to cellular efflux mechanisms) and is not an inhibitor of CYP enzymes, suggesting a very low risk of drug-drug interactions. Finally, Compound 1 has good drug-likeness with 0 violations of Lipinski's Rule of Five and good Bioavailability Score of 0.55. From the medicinal chemistry perspective, the lack of PAINS alerts confirms the lack of non-specific assay interference, and the Synthetic Accessibility score of 2.80 suggests a high ease of synthesis for future development.

Table 7. Physicochemical, pharmacokinetic, and drug-likeness properties of ($C_6H_6O_4$).

Parameter	Category	Value	Interpretation
Physicochemical	Molecular Weight	142.11 g/mol	Ideal (< 500 Da)
	TPSA	70.67 Å²	High Oral Bioavailability
	Rotatable Bonds	1	High Structural Rigidity
Lipophilicity	Consensus Log Po/w	-0.04	Optimal Hydro-Lipophilic Balance
Water Solubility	Log S (ESOL)	-0.70	Very Soluble
Pharmacokinetics	GI Absorption	High	Excellent Absorption
	BBB Permeant	No	Low CNS Toxicity Risk
	P-gp substrate	No	Not Susceptible to Efflux
	CYP Inhibitors	No (All)	Low Drug-Drug Interaction Risk
Druglikeness	Lipinski Rule	Yes	0 Violation
	Bioavailability Score	0.55	Good Bioavailability
Medicinal Chem.	PAINS Alert	0 Alert	No Non-specific Interference
	Synthetic Accessibility	2.80	High Ease of Synthesis

To verify these computational hypotheses, in vitro biological assays were performed with the purified compound 1, as shown in table 8. The IC_{50} value of the isolated metabolite is 70 µg/mL. This scavenging potential strongly supports the stable binding affinities observed against core oxidative regulators such as Peroxiredoxin 5 (4K7O) and Lipoxygenase (1DGH). Furthermore, the in vitro antibacterial screening corroborated the multi-targeted computational predictions, showing moderate growth inhibition against both Gram-positive and Gram-negative pathogens. Minimum Inhibitory Concentration (MIC) of compound 1 was 125µg/mL against *Escherichia coli* and *Salmonella typhi* and 250µg/mL against *Staphylococcus aureus* and *Bacillus subtilis.* The phenotypic susceptibility of *S. aureus* directly supports the high affinity targeting of its essential Tyrosyl-tRNA Synthetase (1JIJ) as predicted in silico. Together, the correlation of the molecular docking parameters, good ADMET profile, and conclusive *in vitro* findings, confirm the significant potential of this 2-pyrone derivative isolated from *Nypa fruticans* endophytic fungi as a dual-action therapeutic scaffold.

Table 8. Antibacterial and antioxidant properties of the pure compound isolated from Nb3

Sample	MIC Value (µg/mL)				IC_{50} (µg/mL)
	E. coli	*S. aureus*	*S. thypi*	*B. subtilis*	
Compound 1	125	250	125	250	70

The presence of a 2-pyrone core backbone in this metabolite is highly significant, as this class of six-membered cyclic unsaturated esters is well-documented to play vital roles in microbial and plant defense mechanisms, chemical signaling, and ecological adaptations [32]. The former study on the *Aspergillus flavus* isolate emphasised the pharmacological importance of this compound as a potential ligand for the GPR12 receptor to induce cAMP production, but the present work broadens the functional diversity of this oxygenated scaffold from *Nypa fruticans* endophytic fungi. By using automated *in silico* workflows to evaluate its multi-target interaction profiles, we demonstrate that the compact and rigid molecular architecture of compound 1 has strong theoretical binding capacities towards key bacterial and oxidative enzymes, establishing its potential as a promising multi-targeted antibacterial and anti-tyrosinase scaffold. Although Compound **1** demonstrated potent antibacterial activity against standard pathogenic strains, further evaluations targeting multidrug-resistant (MDR) clinical isolates and bio-film forming pathogens are warranted to fully determine its potential in combating resistant infections.

Conclusions

Bio-guided screening of endophytic fungi from *Nypa fruticans* led to the identification of *Diaporthe* sp. (Nb3) as a potent source of natural bioactives. Chromatographic purification of its active extract yielded 5-hydroxy-4-(hydroxymethyl)-2H-pyran-2-one (compound 1). Compound 1 showed good antioxidant

activity (IC_{50} = 70 µg/mL) and moderate broad-spectrum antibacterial efficacy against *E. coli*, *S. typhi*, *S. aureus*, and *B. subtilis* (MIC= 125- 250 µg/mL). Note that the crude extract was more potent than the isolated compound and suggests strong synergistic interaction of the secondary metabolites in the extract. The findings were further supported by *in silico* profiling of compound 1, which showed excellent drug-likeness, zero Lipinski violations, favourable ADMET parameters and spontaneous binding affinity toward key target proteins (e.g. Tyrosyl-tRNA Synthetase and Lipoxygenase). In brief, these results establish *Diaporthe* sp. from *Nypa fruticans* as a promising candidate for standardised natural antioxidants, and therapeutic lead development.

Conflicts of Interest

The authors declare that there is no conflict of interest regarding the publication of this paper.

Acknowledgment

The authors would like to express their gratitude to the Directorate of Research and Community Service, Directorate General of Research and Development, Ministry of Higher Education, Science, and Technology for funding and supporting this research under the Penelitian Pendidikan Magister menuju Doktor untuk Sarjana Unggul (PMDSU) program, pursuant to Contract Number: 109/C3/DT.05.00/PL/2025

References

[1] S. K. Ahmed *et al.*, “Antimicrobial resistance: Impacts, challenges, and future prospects,” *J. Med. Surgery, Public Heal.*, vol. 2, no. March, p. 100081, 2024, doi: 10.1016/j.glmedi.2024.100081.
[2] T. R. Walsh, A. C. Gales, R. Laxminarayan, and P. C. Dodd, “Antimicrobial Resistance: Addressing a Global Threat to Humanity,” *PLoS Med.*, vol. 20, no. 7 July, pp. 12–15, 2023, doi: 10.1371/journal.pmed.1004264.
[3] I. Frost, A. Balachandran, S. Paulin-Deschenaux, H. Sati, and M. Hasso-Agopsowicz, “The approach of World Health Organization to articulate the role and assure impact of vaccines against antimicrobial resistance,” *Hum. Vaccines Immunother.*, vol. 18, no. 6, pp. 0–4, 2022, doi: 10.1080/21645515.2022.2145069.
[4] C. S. Ho *et al.*, “Antimicrobial resistance: a concise update,” *The Lancet Microbe*, vol. 6, no. 1, pp. 1–14, 2025, doi: 10.1016/j.lanmic.2024.07.010.
[5] T. B. Tufa, F. Regassa, K. Amenu, J. A. Stegeman, and H. Hogeveen, “Livestock producers’ knowledge, attitude, and behavior (KAB) regarding antimicrobial use in Ethiopia,” *Front. Vet. Sci.*, vol. 10, pp. 1–20, 2023, doi: 10.3389/fvets.2023.1167847.
[6] C. E. Flynn and J. Guarner, “Emerging Antimicrobial Resistance,” *Mod. Pathol.*, vol. 36, no. 9, p. 100249, 2023, doi: 10.1016/j.modpat.2023.100249.
[7] F. O. Ohiagu, P. C. Chikezie, T. O. Maduka, C. M. Chikezie, O. Nwaiwu, and K. R. Paudel, “Antioxidants, Radical Scavengers, and Their Impact on Oxidative Stress,” *Free Radicals Antioxidants*, vol. 14, no. 2, pp. 62–85, 2025, doi: 10.5530/fra.2024.2.7.
[8] İ. Gulcin, *Antioxidants: a comprehensive review*, vol. 99, no. 5. 2025. doi: 10.1007/s00204-025-03997-2.
[9] S. T. Omaye, “Antioxidants: Looking forward after a decade,” *Antioxidants*, vol. 10, no. 12, 2021, doi: 10.3390/antiox10121992.
[10] J. Flieger, W. Flieger, and J. Baj, “Antioxidants : Classification , Natural Sources , Activity / Capacity,” *Materials (Basel).*, vol. 14, no. 4135, pp. 1–54, 2021, [Online]. Available: https://www.mdpi.com/journal/materials
[11] M. E. Rusu, I. Fizeșan, L. Vlase, and D. S. Popa, “Antioxidants in Age-Related Diseases and Anti-Aging Strategies,” *Antioxidants*, vol. 11, no. 10, pp. 1–5, 2022, doi: 10.3390/antiox11101868.
[12] B. Alam *et al.*, “Endophytic Fungi: From Symbiosis to Secondary Metabolite Communications or Vice Versa?,” *Front. Plant Sci.*, vol. 12, no. December, pp. 1–24, 2021, doi: 10.3389/fpls.2021.791033.
[13] Q. xi Li, F. cheng Lin, and Z. zhu Su, “Endophytic fungi-Big player in plant-microbe symbiosis,” *Curr. Plant Biol.*, vol. 42, no. April, p. 100481, 2025, doi: 10.1016/j.cpb.2025.100481.
[14] J. Wen *et al.*, “Endophytic Fungi: An Effective Alternative Source of Plant-Derived Bioactive Compounds for Pharmacological Studies,” *J. Fungi*, vol. 8, no. 2, 2022, doi: 10.3390/jof8020205.
[15] C. Liao *et al.*, *Challenges and update on fungal endophytes: classification, definition, diversity, ecology, evolution and functions*, vol. 131, no. 1. Springer Netherlands, 2025. doi: 10.1007/s13225-025-00550-5.
[16] M. Zhang, C. Zhong, X. Lv, Z. Fang, C. Cheng, and J. Hao, “Germplasm Resource Status and Seed Adaptability of Nypa fruticans Wurmb, an Endangered Species in China,” *Forests*, vol. 15, no. 8, pp. 1–16, 2024, doi: 10.3390/f15081396.
[17] G. D. Nugroho *et al.*, “Review: Phytochemical composition, medicinal uses and other utilization of Nypa fruticans,” *Int. J. Bonorowo Wetl.*, vol. 10, no. 1, pp. 51–65, 2022, doi: 10.13057/bonorowo/w100105.
[18] S. S. A. Nasution, Elfita, H. Widjajanti, and Ferlinahayati, “Diversity, bioactivity, and phytochemistry of endophytic fungi in various organs of nipa palm (Nypa fruticans) mangrove,” *Biodiversitas*, vol. 25, no. 10, pp. 3928–3942, 2024, doi: 10.13057/biodiv/d251053.
[19] A. Loilong, J. Sakayaroj, N. Rungjindamai, R. Choeyklin, and E. B. G. Jones, “Biodiversity of fungi on the palm Nypa fruticans,” *Mar. Fungi Fungal-like Org.*, pp. 273–290, 2012, doi: 10.1515/9783110264067.273.
[20] P. Toppo, P. Jangir, N. Mehra, R. Kapoor, and P. Mathur, “Bioprospecting of endophytic fungi from medicinal plant Anisomeles indica L. for their diverse role in agricultural and industrial sectors,” *Sci. Rep.*, vol. 14, no. 1,

pp. 1–18, 2024, doi: 10.1038/s41598-023-51057-5.
[21] N. H. Caicedo, A. F. Davalos, P. A. Puente, A. Y. Rodríguez, and P. A. Caicedo, "Antioxidant activity of exo-metabolites produced by Fusarium oxysporum: An endophytic fungus isolated from leaves of Otoba gracilipes," *Microbiologyopen*, vol. 8, no. 10, pp. 1–7, 2019, doi: 10.1002/mbo3.903.
[22] E. Charria-Girón *et al.*, "Evaluation of the Antibacterial Activity of Crude Extracts Obtained From Cultivation of Native Endophytic Fungi Belonging to a Tropical Montane Rainforest in Colombia," *Front. Microbiol.*, vol. 12, no. September, 2021, doi: 10.3389/fmicb.2021.716523.
[23] T. Watanabe, *Pictorial Atlas of Soil and Seed Fungi*. 2010. doi: 10.1201/ebk1439804193.
[24] D. H. Larone, L. F. Westblade, E. M. Burd, S. R. Lockhart, G. W. Procop, and T. J. Walsh, *Larone's medically important fungi: A guide to identification (7th ed.)*. John Wiley & Sons, 2023. doi: 10.1128/9781555819880.
[25] L. LaPierre, "Antimicrobial Susceptibility Testing Laboratory Guide : Methodologies for," *APEC Proj. CTI 24 2017A*, no. May, pp. 1–19, 2020.
[26] S. Baliyan *et al.*, "Determination of Antioxidants by DPPH Radical Scavenging Activity and Quantitative Phytochemical Analysis of Ficus religiosa," *Molecules*, vol. 27, no. 4, 2022, doi: 10.3390/molecules27041326.
[27] S. Dallakyan and A. J. Olson, "Small-Molecule Library Screening by Docking with PyRx," vol. 1263, pp. 243–250, 2015, doi: 10.1007/978-1-4939-2269-7.
[28] L. Schrödinger, "The PyMOL Molecular Graphics System, Version 3.0," 2023.
[29] D. S. BIOVIA, "Discovery Studio Modeling Environment," 2025, *Dassault Systèmes, San Diego*.
[30] B. Kowalska-Krochmal and R. Dudek-Wicher, "The minimum inhibitory concentration of antibiotics: Methods, interpretation, clinical relevance," *Pathogens*, vol. 10, no. 2, pp. 1–21, 2021, doi: 10.3390/pathogens10020165.
[31] Elfita, R. Oktiansyah, Mardiyanto, H. Widjajanti, A. Setiawan, and S. S. A. Nasution, "Bioactive Compounds of Endophytic Fungi Lasiodiplodia theobromae Isolated From The Leaves of Sungkai (*Peronema canescens*)," *Biointerface Res. Appl. Chem.*, vol. 13, no. 6, Dec. 2023, doi: 10.33263/BRIAC136.530.
[32] A. Lin, X. Lu, Y. Fang, T. Zhu, Q. Gu, and W. Zhu, "NOTE Two New 5-Hydroxy-2-pyrone Derivatives Isolated from a Marine-derived Fungus Aspergillus flavus," vol. 61, no. 4, pp. 245–249, 2008.
[33] A. N. M. Gubran and M. Ali, "Narrative review : Cell wall synthesis inhibitors with an emphasis on mode of actions , resistance mechanisms , and clinical utility and dosages," *The Microbe*, vol. 11, no. March, p. 100700, 2026, doi: 10.1016/j.microb.2026.100700.
[34] A. Yadav and R. K. Salar, "Next Nanotechnology Tyrosinase inhibitors : Molecular mechanisms , therapeutic potentials , and translational applications in dermatology and beyond," *Next Nanotechnol.*, vol. 9, no. February, p. 100452, 2026, doi: 10.1016/j.nxnano.2026.100452.
[35] X. Qiu *et al.*, "Crystal structure of Staphylococcus aureus tyrosyl-tRNA synthetase in complex with a class of potent and specific inhibitors," no. 2001, pp. 2008–2016, 2016, doi: 10.1101/ps.18001.).
[36] N. Schormann *et al.*, "The catalytic domains of Streptococcus mutans glucosyltransferases : a structural analysis research communications," pp. 119–127, 2023, doi: 10.1107/S2053230X23003199.
[37] X. Li *et al.*, "Bioorganic & Medicinal Chemistry Letters Structure-based design of new DHFR-based antibacterial agents :," *Bioorg. Med. Chem. Lett.*, vol. 21, no. 18, pp. 5171–5176, 2011, doi: 10.1016/j.bmcl.2011.07.059.
[38] W. Deng and C. L. M. J. V. Verlinde, "Evaluation of Different Virtual Screening Programs for Docking in a Charged Binding Pocket," *J. Chem. Inf. Model.*, vol. 48, no. 10, pp. 2010–2020, 2008, doi: 10.1021/ci800154w.Evaluation.
[39] N. Bernardo-garcia *et al.*, "Allostery , Recognition of Nascent Peptidoglycan and Crosslinking of the Cell Wall by the Essential Penicillin- Binding Protein 2x of Streptococcus pneumoniae Allostery , Recognition of Nascent Peptidoglycan and Crosslinking of the Cell Wall by the Essent," *ACS Chem. Biol.*, 2018, doi: 10.1021/acschembio.7b00817.
[40] P. Panchaud *et al.*, "Discovery and Optimization of Isoquinoline Ethyl Ureas as Antibacterial Agents," *J. Med. Chem.*, 2017, doi: 10.1021/acs.jmedchem.6b01834.
[41] C. . Kavanagh, K.L.; Johansson, C.; Papagrigoriou, E.; Kochan, G.; Umeano, M. . Gileadi, O.; von Delft, F.; Weigelt, J.; Arrowsmith, C.H.; Sundstrom, and U. . S. G. C. (SGC) Edwards, A.; Oppermann, "Crystal structure of human glutathione peroxidase 7," 2007.
[42] C. Aguirre, T. ten Brink, J.-F. Guichou, O. Cala, and I. Krimm, "Comparing Binding Modes of Analogous Fragments Using NMR in Fragment-Based Drug Design : Application to PRDX5," vol. 9, no. 7, pp. 1–11, 2014, doi: 10.1371/journal.pone.0102300.
[43] C. D. Putnam, A. S. Arvai, Y. Bourne, J. A. Tainer, and J. Aiguier, "Active and Inhibited Human Catalase Structures : Ligand and NADPH Binding and Catalytic Mechanism," 2000.
[44] S. N. Savvides and P. A. Karplus, "Kinetics and Crystallographic Analysis of Human Glutathione Reductase in Complex with a Xanthene Inhibitor *," *J. Biol. Chem.*, vol. 271, no. 14, pp. 8101–8107, 1996, doi: 10.1074/jbc.271.14.8101.
[45] H. tae Kim, H. Cha, and K. Y. Hwang, "Structural insight into the inhibition of carbonic anhydrase by the COX-2-selective inhibitor polmacoxib (CG100649)," *Biochem. Biophys. Res. Commun.*, vol. 478, no. 1, pp. 1–6, 2016, doi: 10.1016/j.bbrc.2016.07.114.
[46] T. Saito *et al.*, "p62/Sqstm1 promotes malignancy of HCV-positive hepatocellular carcinoma through Nrf2-dependent metabolic reprogramming," *Nat. Commun.*, 2016, doi: 10.1038/ncomms12030.